ISSN 1810-2328, Journal of Engineering Thermophysics, 2017, Vol. 26, No. 4, pp. 514–531. © Pleiades Publishing, Ltd., 2017.

Effect of Relative Camber on the Aerodynamic Performance Improvement of Asymmetrical Blunt Trailing-Edge Modification

X. Zhang[1,2*], G. G. Wang[1], M. J. Zhang[1], and W. Li[3]

[1] *Tianjin Key Laboratory of Advanced Mechatronics Equipment Technology, Tianjin Polytechnic University, Tianjin, 300387 China*

[2] *State Key Laboratory of Building Safety and Built Environment, Beijing, 100013 China*

[3] *School of Energy and Safety Engineering, Tianjin Chengjian University, Tianjin, 300384 China*

Received December 16, 2016

Abstract—In this paper, the aerodynamic performance of the S series of wind turbine airfoils with different relative cambers and their modifications is numerically studied to facilitate a greater understanding of the effects of relative camber on the aerodynamic performance improvement of asymmetrical blunt trailing-edge modification. The mathematical expression of the blunt trailing-edge modification profile is established using the cubic spline function, and S812, S816 and S830 airfoils are modified to be asymmetrical blunt trailing-edge airfoils with different thicknesses. The prediction capabilities of two turbulence models, the k-ω SST model and the S-A model, are assessed. It is observed that the k-ω SST model predicts the lift and drag coefficients of S812 airfoil more accurately through comparison with experimental data. The best trailing-edge thickness and thickness distribution ratio are obtained by comparing the aerodynamic performance of the modifications with different trailing-edge thicknesses and distribution ratios. It is, furthermore, investigated that the aerodynamic performance of original airfoils and their modifications with the best thickness of 2% c and distribution ratio being 0:4 so as to analyze the increments of lift and drag coefficients and lift–drag ratio. Results indicate that with the increase of relative camber, there are relatively small differences in the lift coefficient increments of airfoils whose relative cambers are less than 1.81%, and the lift coefficient increment of airfoil with the relative camber more than 1.81% obviously decreases for the angle of attack less than 6.3°. The drag coefficient increment of S830 airfoil is higher than that of S816 airfoil, and those of these two airfoils mainly decrease with the angle of attack. The average lift–drag ratio increment of S816 airfoil with the relative camber of 1.81% at different angles of attack ranging from 0.1° to 20.2° is the largest, closely followed by S812 airfoil. The lift–drag ratio increment of S830 airfoil is negative as the angle of attack exceeds 0.1°. Thus, the airfoil with medium camber is more suited to the asymmetrical blunt trailing-edge modification.

DOI: 10.1134/S1810232817040075

1. INTRODUCTION

The wind turbine blade is the major component used to capture wind energy, and the aerodynamic performance of airfoil directly affects the utilization rate of wind energy. Moreover, with the increase of the dimensions of wind turbine, the requirement on strength of blade under the harsh operating environment is also increased in recent years. The structural performance of blade can be improved through the thick airfoil used in the inboard region, near the root of the blade, because the thick airfoil can support large flapwise bending loads [1–3]. However, the aerodynamic performance of thick airfoil is usually poor. In order to improve the structural and aerodynamic performance of a large-scale wind turbine blade, the blunt trailing-edge structure is adopted [4]. The blunt trailing-edge airfoil with the larger trailing-edge thickness and cross-section area not only improves the airfoil's ability to resist bending and torsion, but it also has a great improvement in the lift and makes the lift less sensitive to the leading-edge roughness [5].

*E-mail: zhangxu@tjpu.edu.cn

Baker et al. [6] analyzed the aerodynamic performance of symmetric blunt trailing-edge airfoils through the experimental method. Standish et al. [7] used a viscous/inviscid interaction method and three Reynolds-averaged Navier–Stokes methods to investigate the blunt trailing-edge airfoil. Ronit et al. [8, 9] studied the design and parameters of a new low Reynolds number flatback airfoil, and the performance of this airfoil by experimentation, computational fluid dynamics (CFD) analysis, and PIV. Chao et al. [10] numerically analyzed the effects of modifying the inboard portion of the experimental NREL Phase VI rotor with a thickened blunt trailing-edge version of S809 airfoil. Deng et al. [11] calculated the aerodynamic performance of blunt trailing-edge airfoils designed by directly cutting off the trailing-edge, symmetrically or asymmetrically adding the thickness and rotating the airfoil plane. Xu et al. [12] and Li et al. [13] conducted the numerical simulation to analyze the aerodynamic characteristics of many airfoils before and after adding the trailing-edge thickness. Yang et al. [1] presented the design and prediction of four large-thickness airfoils with blunt trailing-edge. The above research results indicate that the blunt trailing-edge blade profile increases the lift coefficient and the lift–drag ratio, and is viable as a bridge to connect structural requirements with aerodynamic performance in designing future wind turbine rotors. However, it can be seen that the previous studies on thickening airfoil's trailing-edge are largely focused on some particular airfoils, and the effects of adding the trailing-edge thickness asymmetrically on the aerodynamic performance improvement of a certain series of wind turbine airfoils are investigated rarely.

It is generally known that wind turbine belongs to the prime mover, also known as a turbine. The energy conversion capability of the turbine is greater than that of the compressor because the camber of turbine blade profile is much larger than that of compressor blade. But the traditional wind turbine always adopts the propeller airfoil belonging to the compressor, which seriously affects the ability of wind turbine to absorb wind energy [14, 15]. It can be observed that the aerodynamic performance improvement of wind turbine blade is also related to the relative camber of airfoil prototype.

Many researchers have numerically and experimentally investigated the effect of relative camber on the aerodynamic performance of airfoil. Larsen et al. [16] presented a model for determining the dynamic lift coefficient of a wind turbine profile, and analyzed the influence of camber and thickness distribution on the backbone curve. Shen et al. [14, 15] modified the airfoil FFA-W3-211 toward the turbine-like airfoil in order to increase the camber of pressure surface, and conducted a number of comparative experiments of wind turbine with original or modified airfoils in a small low-speed tunnel. Li et al. [17] used the numerical simulation to research the effect of relative camber on the aerodynamic characteristics of wind turbine airfoil. The computational and experimental results show that within a certain range of relative camber, the large camber airfoil has higher lift and drag coefficients and lift–drag ratio. According to the previous researches on the effects of blunt trailing-edge modification and relative camber on the airfoil aerodynamic performance, it can be seen that this two problems have been discussed separately. Few literatures investigate the effect of the relative camber on the aerodynamic performance of wind turbine airfoil with the trailing-edge thickness added asymmetrically.

In the second part of this study, the asymmetrical blunt trailing-edge modification formula has been established using the cubic spline function, and the S series of dedicated wind turbine airfoils with different relative cambers from National Renewable Energy Laboratory (NREL) are modified to be asymmetrical blunt trailing-edge airfoils. This third part is essentially devoted to comparing the numerical results of S812 airfoil with experimental data on the one hand, and to a detailed assessment of the calculation accuracy of CFD on the other hand. Section 4 then analyzes the best trailing-edge thickness and distribution ratio by comparison of the aerodynamic performance of asymmetrical blunt trailing-edge airfoils. The next step, Section 5, is the investigation of the effect of relative camber on the aerodynamic performance improvement of asymmetrical blunt trailing-edge modification with the best trailing-edge thickness and distribution ratio. The investigated results can provide a reference for the optimization design of wind turbine airfoil.

2. MATHEMATICAL EXPRESSION OF BLUNT TRAILING-EDGE AIRFOIL

For S812, S816, and S830 airfoils, the maximum relative thickness is 21% and occurs at 39% c, and the relative camber, located at 77% c, 68% c, and 70% c, is 1.57%, 1.81%, and 4.46%, respectively, where c is the chord length of the airfoil. S812 airfoil is modified from the maximum relative thickness position, while, relative thickness and its position, relative camber and chord length remain unchanged.

According to [18], the effects of different smooth curves from the maximum thickness position to the trailing-edge point on the airfoil aerodynamic performance are very small. Thus, the mathematical expression of the blunt trailing-edge modification profile is established using the cubic spline function that can work well to guarantee the smoothness and continuity of the curve. The prototype profile and blunt trailing-edge modification schematic of S812 airfoil are shown in Fig. 1.

The coordinates of some control point z_i on the original airfoil are (x_i, y_i), where i denotes the upper

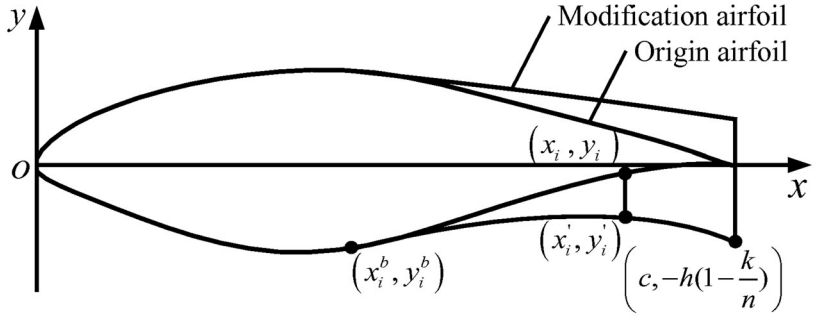

Fig. 1. S812 airfoil prototype and blending curve design.

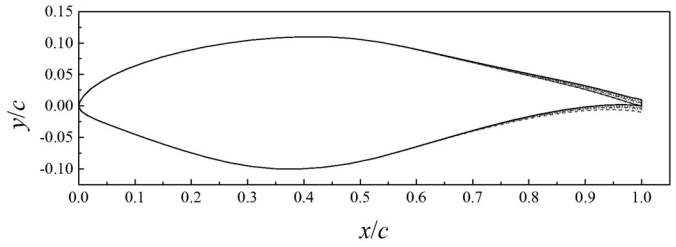

(a) S812, $h = 1\%\, c$

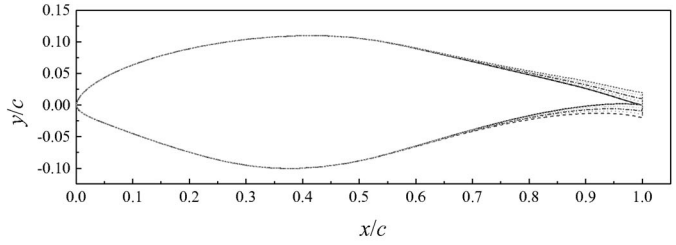

(b) S812, $h = 2\%\, c$

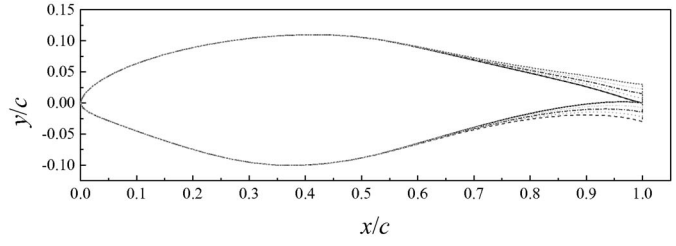

(c) S812, $h = 3\%\, c$

Fig. 2. Profiles of S812, S816, and S830 airfoils and their modifications. — Origin airfoil, – – – – $k/(n-k) = 0:4$, · · · · · $k/(n-k) = 1:3$, -·-·-·- $k/(n-k) = 2:2$, – · · – · · – $k/(n-k) = 3:1$, - - - - $k/(n-k) = 4:0$.

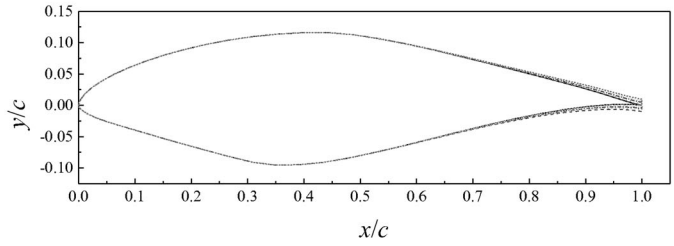

(d) S816, $h = 1\%\ c$

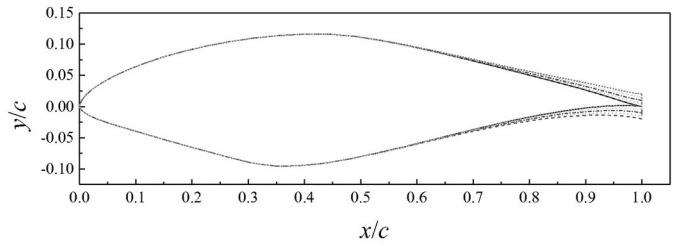

(e) S816, $h = 2\%\ c$

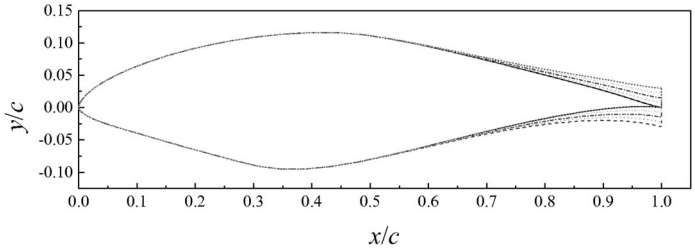

(f) S816, $h = 3\%\ c$

Fig. 2. (Contd.)

or lower surfaces and is 1 or 2, respectively. After the original airfoil is modified, the new coordinates of the same control point expressed as z_i' are (x_i', y_i'), and the coordinate expressions are as follows:

$$x_i' = x_i,$$

$$y_i' = \begin{cases} y_i + h\dfrac{k}{n}\left(\dfrac{x_i - x_i^b}{c - x_i^b}\right)^3, & i = 1,\ \ k = 0, 1, \ldots, n, \\ y_i - h\left(1 - \dfrac{k}{n}\right)\left(\dfrac{x_i - x_i^b}{c - x_i^b}\right)^3, & i = 2,\ \ k = 0, 1, \ldots, n, \end{cases} \tag{1}$$

where h is the trailing-edge thickness, (x_i^b, y_i^b) is the coordinates of maximum thickness position on the airfoil surface, and k/n is the ratio of trailing-edge thickness of the upper surface to that of airfoil.

The ratio of trailing-edge thickness of the upper surface to that of the lower surface beside the central camber line $k/(n-k)$ is the trailing-edge thickness distribution ratio. According to the distribution ratio being 0:4, 1:3, 2:2, 3:1, and 4:0, the asymmetric blunt trailing-edge modification profiles of S812, S816, and S830 airfoils, as shown in Fig. 2, are obtained using Eq. (1), when the trailing-edge thickness is $1\%\ c$, $2\%\ c$, and $3\%\ c$, respectively. In this present study, modified airfoils with the above five distribution ratios are expressed as follows: airfoil_0, airfoil_1, airfoil_2, airfoil_3, and airfoil_4, in that order.

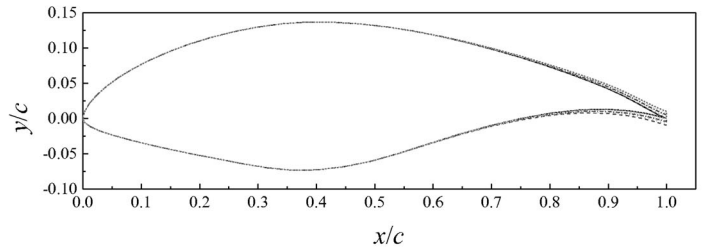

(g) S830, $h = 1\%\ c$

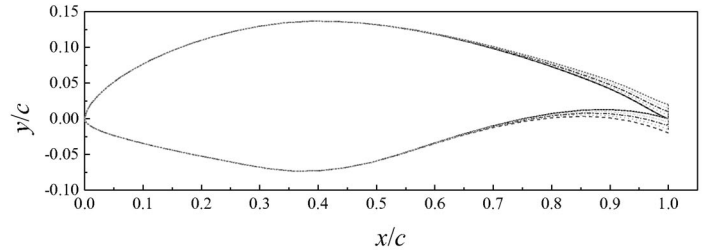

(h) S830, $h = 2\%\ c$

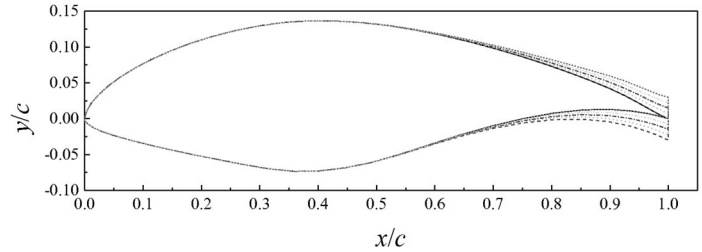

(i) S830, $h = 3\%\ c$

Fig. 2. (Contd.)

3. MATHEMATICAL MODEL AND NUMERICAL METHOD

In this section, the detailed computation treatments and algorithms are explained as follows:

3.1. Numerical Scheme

The flow field calculation performs the steady-state numerical simulation method in the present study, which simplifies continuity and momentum equations by eliminating the time marching [19–21]. The higher precision turbulence model chosen by experimental validation is used to close the governing equations. The convection term is discretized using the second-order upwind difference scheme to improve the solution accuracy and numerical stability, and the implicit pressure-based algorithm SIMPLE is used to solve the pressure–velocity coupling [21]. The commercial CFD software Fluent is employed. Through monitoring the lift and drag coefficients as well as the normalized residuals of all variables, the adequate convergence of the steady-state simulation is ensured. When the convergence criterions of continuity and velocity components are 10^{-3} and 10^{-5}, respectively, and those of k and ω are 10^{-4}, the numerical convergence of the solution can be accepted.

The S series of airfoils developed by NREL are commonly used blade sections of horizontal-axis wind turbine. NREL conducted wind tunnel tests of airfoils in the S series and obtained good-quality aerodynamic data for different angles of attack ranging from $-6.2°$ to $20.2°$ in [22], which offers a good opportunity to examine the capability of CFD simulation.

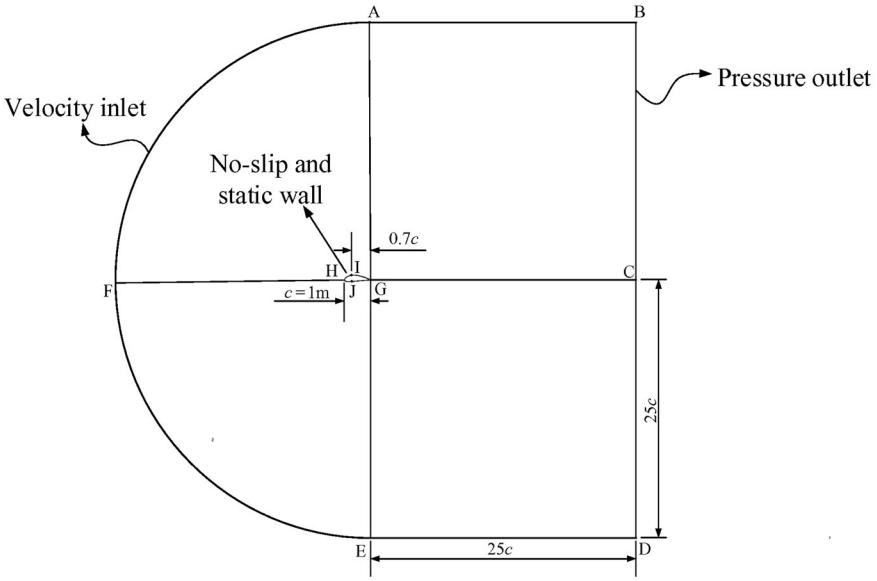

Fig. 3. Computational domain.

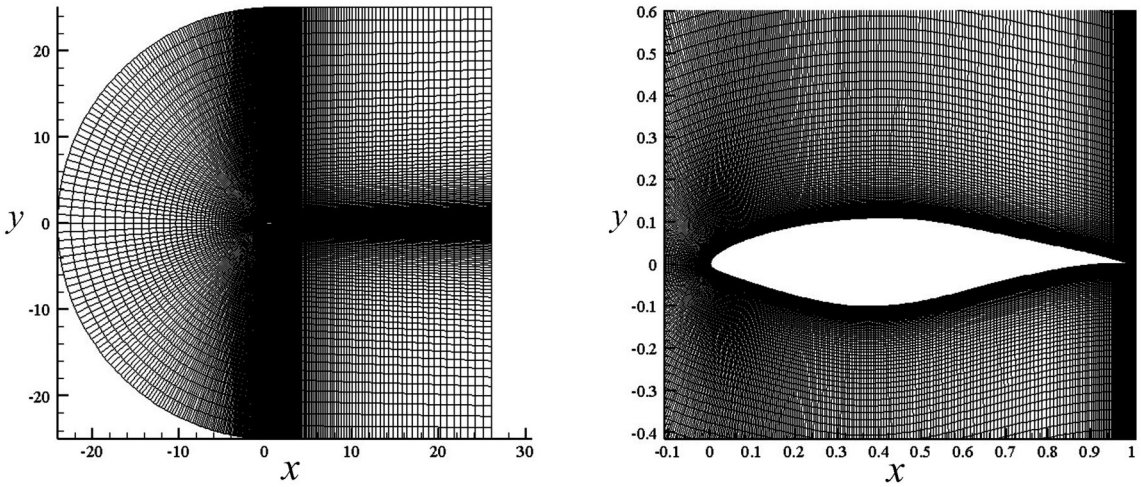

(a) Grid of the airfoil (b) Part grid of the airfoil

Fig. 4. Mesh distribution around the airfoil.

3.2. Computational Mesh

To ensure that the boundary location does not affect the flow, the computational domain in the present study consists of a semicircle domain of diameter $50c$ and a rectangular domain of size $50c \times 25c$, and the airfoil locates near the semicircular center, as shown in Fig. 3. And four faces AFHIG, EFHJG, ABCG, and EDCG are obtained. In order to mesh the four faces separately, the distribution points for each edge of this four faces first need to be defined. Then, each edge is meshed based on the following criteria:

1. We first specify the direction of grid division, the division length at the start of the edge and the interval count, and then the successive ratio is automatically computed by Gambit.

2. We first specify the direction of grid division, the division lengths at the start and the end of the edge and the interval count, and then the successive ratio is automatically computed by Gambit.

3. We create the boundary layer attached to the edges of airfoil, and need to specify the first-row height, the growth factor and the number of rows of boundary layer.

For the first group of the edges HI, HJ, GA, HF, GE, CB, CD, AB, GC, ED, AF, and EF, the second group of the edges IG and JG, and the third group of the edges of airfoil (i.e., HI, IG, HJ, and JG), the mesh division adopts the first, second and third criterion, respectively. After the appropriate edge meshes have been specified, we mesh the faces AFHIG, EFHJG, ABCG, and EDCG.

The computational grid for the simulation of flow around the airfoil is generated using the software of Gambit and is illustrated in Fig. 4a. The stationary domain of airfoil is discretized by a C-type grid mesh, centred on the airfoil. And the near wall grid is refined to assure y^+ is less than 5, as shown in Fig. 4b.

3.3. Boundary Conditions

As can be observed in Fig. 3, the velocity inlet and the pressure outlet are respectively located in the left and right sides of the domain boundary to implement the appropriate boundary conditions. Though specifying the freestream velocity at the velocity inlet, Reynolds number (Re) of 1×10^6 in the simulation is obtained to match the experiment. The atmospheric pressure at the pressure outlet is set to zero. The wall condition is specified for the airfoil surface, and the no-slip and static-wall boundary conditions are applied. And according to [22], the turbulence kinetic energy and the turbulence dissipation rate at the inlet boundary are set to default values in the turbulence specification method of the CFD software Fluent.

3.4. Turbulence Model Comparison and Adaptability Verification

Two turbulence models, the k-ω SST model and the S-A model, are assessed by comparing the prediction results with the experimental data of [22]. The numerical simulation of S812 airfoil is performed when Re is 1×10^6 and Mach number (Ma) is 0.0435, as shown in Fig. 5. Figure 5 shows the calculated values of lift coefficient agree well with the experimental ones for the angle of attack less than 10.1°, and are greater than the experiment ones for the angle of attack more than 10.1°. This is because all turbulence models cannot match the actual physical model very well after stalling. One can also see from Fig. 5 that the numerical results of lift and drag coefficients based on the k-ω SST model are closer to the experiment data for the angle of attack more than 10.1° and ranging from −6.2° to 20.2°, respectively. Overall, the results of numerical computation based on the k-ω SST model are in good agreement with those of experiment. In addition, the research results of [22–24] also indicate that the k-ω SST model is especially suitable for calculating the wake flow field of blunt trailing-edge airfoil. Therefore, the k-ω SST turbulence model is chosen to close the governing equations.

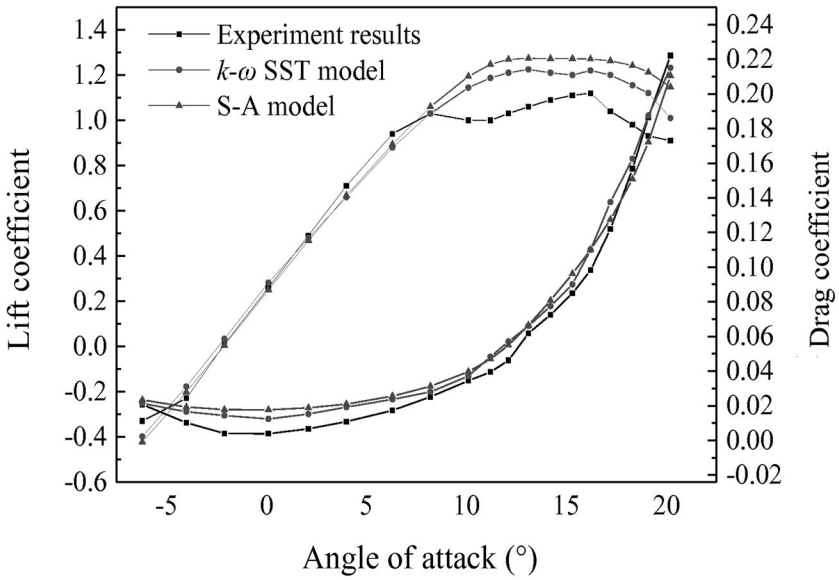

Fig. 5. Comparison of the calculated and experimental results of S812 airfoil.

3.5. Grid Independence Study

A grid independence analysis, that is, the effects of the division length at the start of the edge and the grid number on the numerical result, is performed in preliminary calculations to ensure that the adequate mesh resolution is achieved and the spatial discretization errors are minimal for the simulations in the present work. The lift and drag coefficients and lift–drag ratio of S812 airfoil are calculated for three division lengths at the start of the edge, namely, 0.0003c, 0.0005c, and 0.001c, and for three grid numbers, namely, 91710, 167550, and 233160 cells, respectively, as presented in Figs. 6 and 7.

Figures 6a and 6b show the differences among first division lengths of 0.0003c, 0.0005c, and 0.001c are rather small for the lift and drag coefficients, and lift–drag ratio. One can also see from Figs. 7a and 7b that the mesh with 167550 elements in the domain is sufficient. That said, the grids of 167550 and the

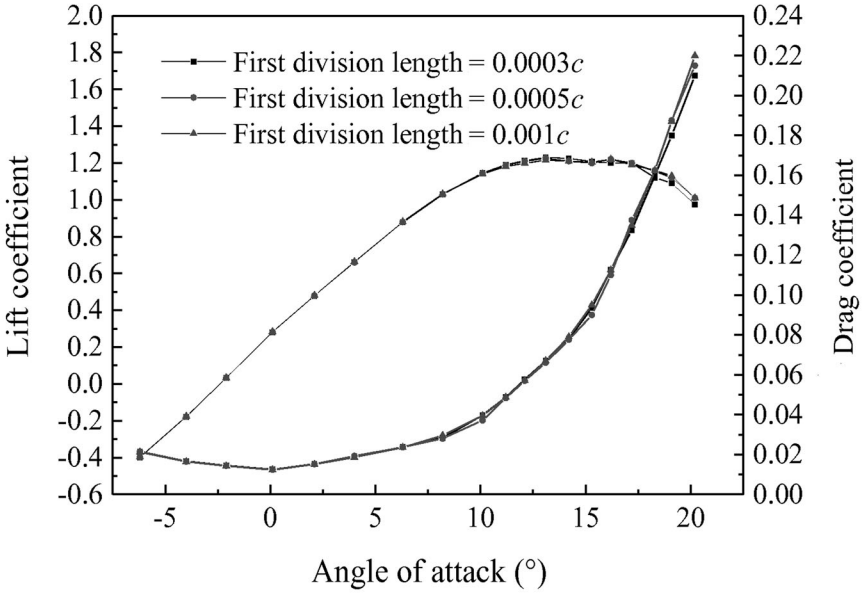

Fig. 6. Edge's first division length dependence of the numerical solution.

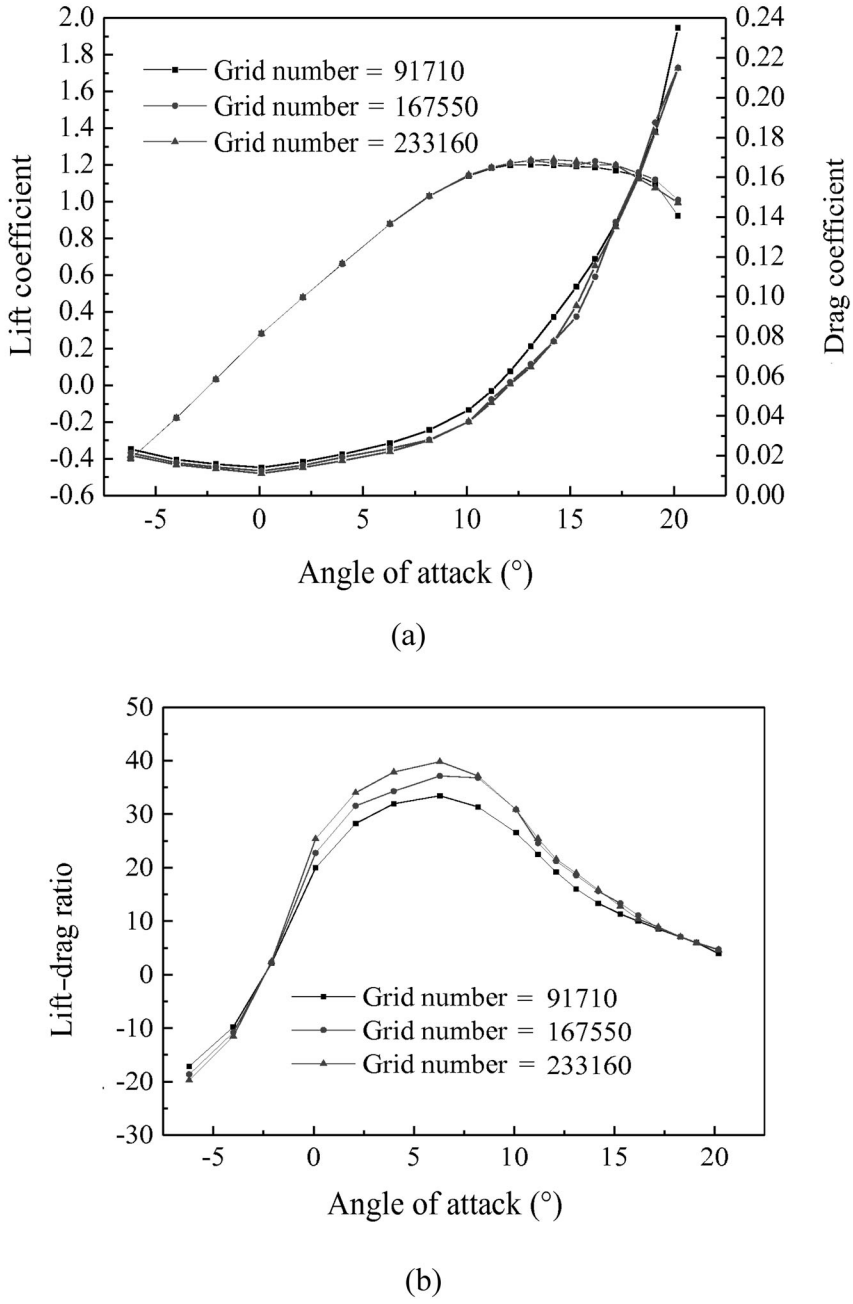

Fig. 7. Grid number dependence of the numerical solution.

first division length of $0.0005c$ are chosen for the further computation, which assures y^+ is about 1. The following tables, namely, Table 1 and Table 2, show the detailed parameters to use for different edges.

4. BEST TRAILING-EDGE THICKNESS AND DISTRIBUTION RATIO

The aerodynamic performance of asymmetrical blunt trailing-edge airfoils with different trailing-edge thicknesses and distribution ratios is investigated to obtain the best trailing-edge thickness and thickness distribution ratio. Lift and drag coefficients, and lift–drag ratios of asymmetrical blunt trailing-edge modifications for S812 airfoil are shown in Fig. 8 and Fig. 9.

According to Fig. 8, the lift and drag coefficients of S812_0, S812_1, and S812_2 airfoils increase with the increase of the trailing-edge thickness, and are all higher than those of original S812 airfoil, but

Table 1. Parameters to use for the different edges

Edges	Direction of grid division	First division length	Last division length	Interval count
HI and HJ	Left to right	$0.0005c$		150
IG and JG	Left to right	$0.005c$	$0.0005c$	140
HF	Right to left	$0.0001c$		170
GA and CB	Upwards	$0.0001c$		170
GE and CD	Downwards	$0.0001c$		170
AB, GC, and ED	Left to right	$0.0005c$		200
AF and EF	Right to left	$0.0005c$		290

Table 2. Parameters to use for the boundary layer

Edges	Direction of grid division	First-row height	Growth factor	Number of rows
HI, IG, HJ, and JG	Outward	$0.0001c$	1	20

the drag coefficients of S812_3 and S812_4 airfoils are very close to that of S812 airfoil. The smaller the trailing-edge thickness of the lower surface is, the less obvious the above change rulers of lift and drag coefficients with the trailing-edge thickness are. In addition, the lift coefficients of S812_4 and S812_3 airfoils are successively smaller than that of S812 airfoil, and decrease with the increase of the trailing-edge thickness as the angle of attack is less than 10.1° and 4°, respectively. The lift coefficient of S812_3 airfoil increases at different angles of attack ranging from 4° to 15.3°, and increases first and then decreases for the angle of attack more than 15.3°, but that of S812_4 airfoil increases as the angle of attack exceeds 10.1°. The lift coefficients of the two modifications are basically smaller than that of S812 airfoil.

One can also see from Fig. 8 that for the same trailing-edge thickness, the lift and drag coefficients of these modifications all decrease with the decrease of the trailing-edge thickness of the lower surface, and the drag coefficient is basically higher than that of S812 airfoil. As the trailing-edge thickness is 1% c, 2% c, and 3% c, respectively, the lift coefficient of S812_3 airfoil is smaller than that of S812 airfoil for the angle of attack less than 0.1°, 2.1°, and 4°, and so does S812_4 airfoil for the angle of attack less than 6.3°, 8.2°, and 10.1°. However, the lift coefficients of this five modified airfoils are all higher than that of S812 airfoil at different angles of attack ranging from 6.3° to 11.2°, 8.2° to 12.1°, and 10.1° to 15.3°. Furthermore, the above change rulers of lift and drag coefficients with the trailing-edge thickness distribution ratio become more obvious as the trailing-edge thickness increases.

Figure 9 shows with the increase of the trailing-edge thickness, the maximum lift–drag ratios of S812_0 and S812_1 airfoils increase first and then decrease, and that of S812_2 airfoil decreases first and then increases, and those of S812_3 and S812_4 airfoils decrease. It can also be observed from Fig. 9 that with the decrease of the trailing-edge thickness of the lower surface, the maximum lift–drag ratios of these modifications do not vary much and are all higher than that of original S812 airfoil for trailing-edge thickness of 1% c, and those of S812_0 and S812_1 airfoils are higher than that of S812 airfoil for the trailing-edge thickness of 2% c, and those of this five modified airfoils decrease and are basically smaller than that of original airfoil for the trailing-edge thickness of 3% c. Through the above analysis, the best trailing-edge thickness and thickness distribution ratio are 2% c and 0:4, respectively.

5. EFFECT OF RELATIVE CAMBER ON AERODYNAMIC PERFORMANCE IMPROVEMENT OF ASYMMETRICAL BLUNT TRAILING-EDGE MODIFICATION

The aerodynamic performance of original airfoils with different relative cambers and their asymmetrical blunt trailing-edge modifications with the best trailing-edge thickness of 2% c and distribution ratio

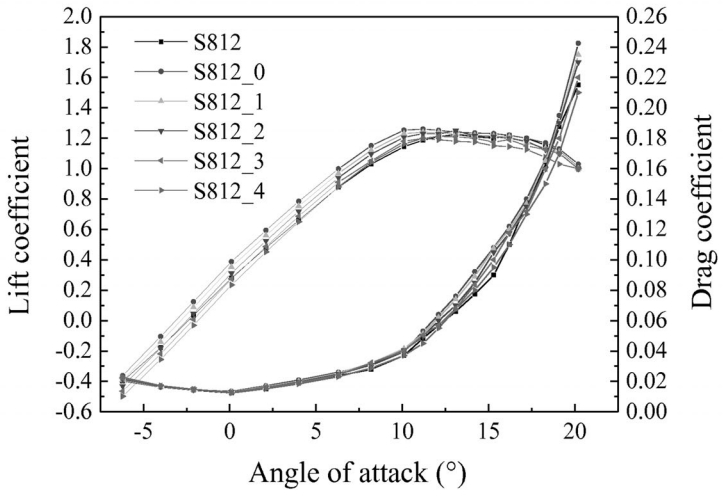

(a) Trailing-edge thickness of 1% *c*

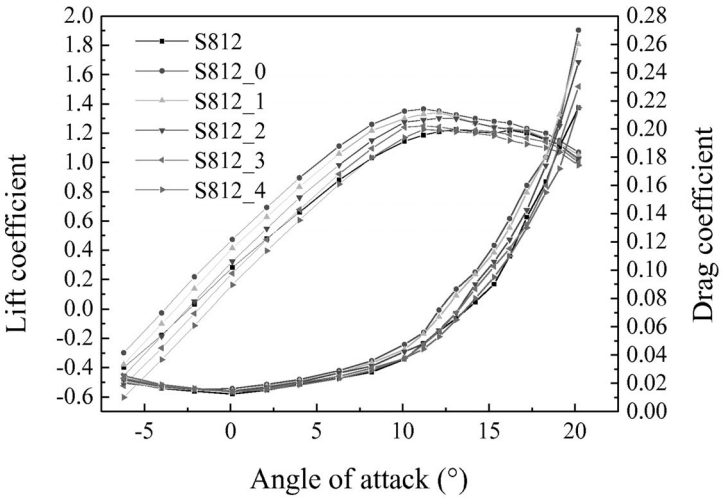

(b) Trailing-edge thickness of 2% *c*

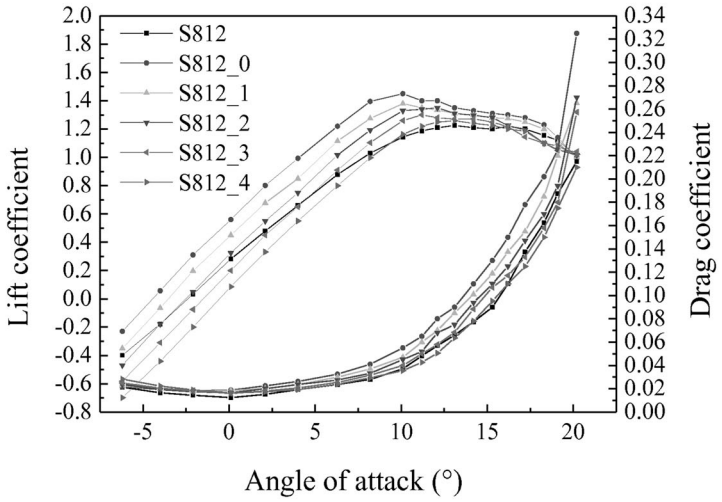

(c) Trailing-edge thickness of 3% *c*

Fig. 8. Lift and drag coefficients of S812 airfoil and its modified airfoils.

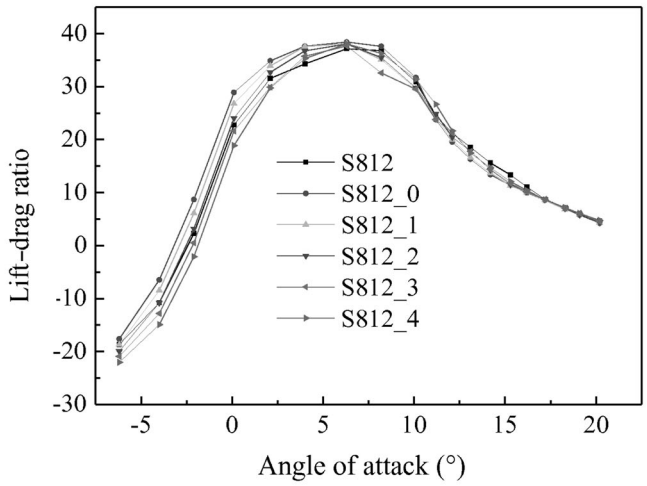

(a) Trailing-edge thickness of 1% c

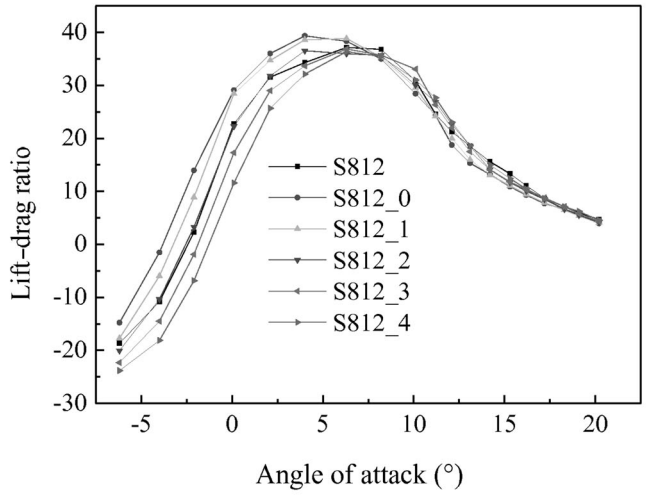

(b) Trailing-edge thickness of 2% c

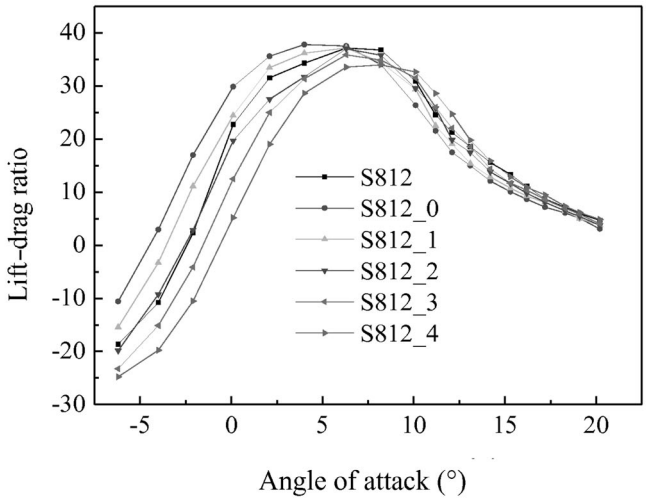

(c) Trailing-edge thickness of 3% c

Fig. 9. Lift–drag ratios of S812 airfoil and its modified airfoils.

being 0:4 is investigated to analyze the effect of relative camber on the lift and drag coefficients, lift–drag ratio, and increments of three parameters.

5.1. Aerodynamic Performance of Airfoils with Different Relative Cambers

The lift and drag coefficients, and lift–drag ratios of airfoil S812, S816, and S830 are studied and shown in Fig. 10. According to Fig. 10a, the lift coefficient increases with the increase of relative camber, so does the drag coefficient at different angles of attack ranging from −2.1° to 17.2°. But the drag coefficients of airfoil S812, S816, and S830 are very close for the angle of attack less than −2.1° and more than 17.2°. In Fig. 10b, the lift–drag ratio increases with the increase of relative camber for the angle of attack less than 6.3°, and decreases first and then increases as the angle of attack exceeds 6.3°.

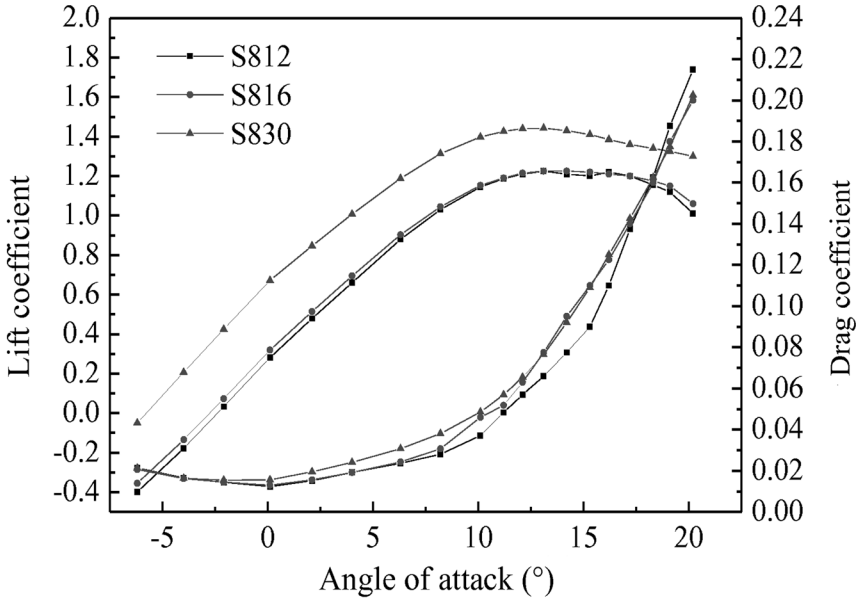

Fig. 10. Results of original airfoils with different relative cambers.

5.2. Aerodynamic Performance of Asymmetrical Blunt Trailing-Edge Modifications of Airfoils with Different Relative Cambers

The lift and drag coefficients, and lift–drag ratios of asymmetrical blunt trailing-edge modifications with the best thickness of 2% c and distribution ratio being 0:4 for S812, S816, and S830 airfoils, are calculated, analyzed and presented in Fig. 11.

Figure 11a shows as the relative camber increases, the lift coefficients of S812_0, S816_0, and S830_0 airfoils increase for the angle of attack less than 10.1°. And the lift coefficient of S812_0 airfoil is no different than that of S816_0 airfoil, and those of these two airfoils are obviously less than that of S830_0 airfoil for the angle of attack more than 10.1°. One can also see from this graph that the drag

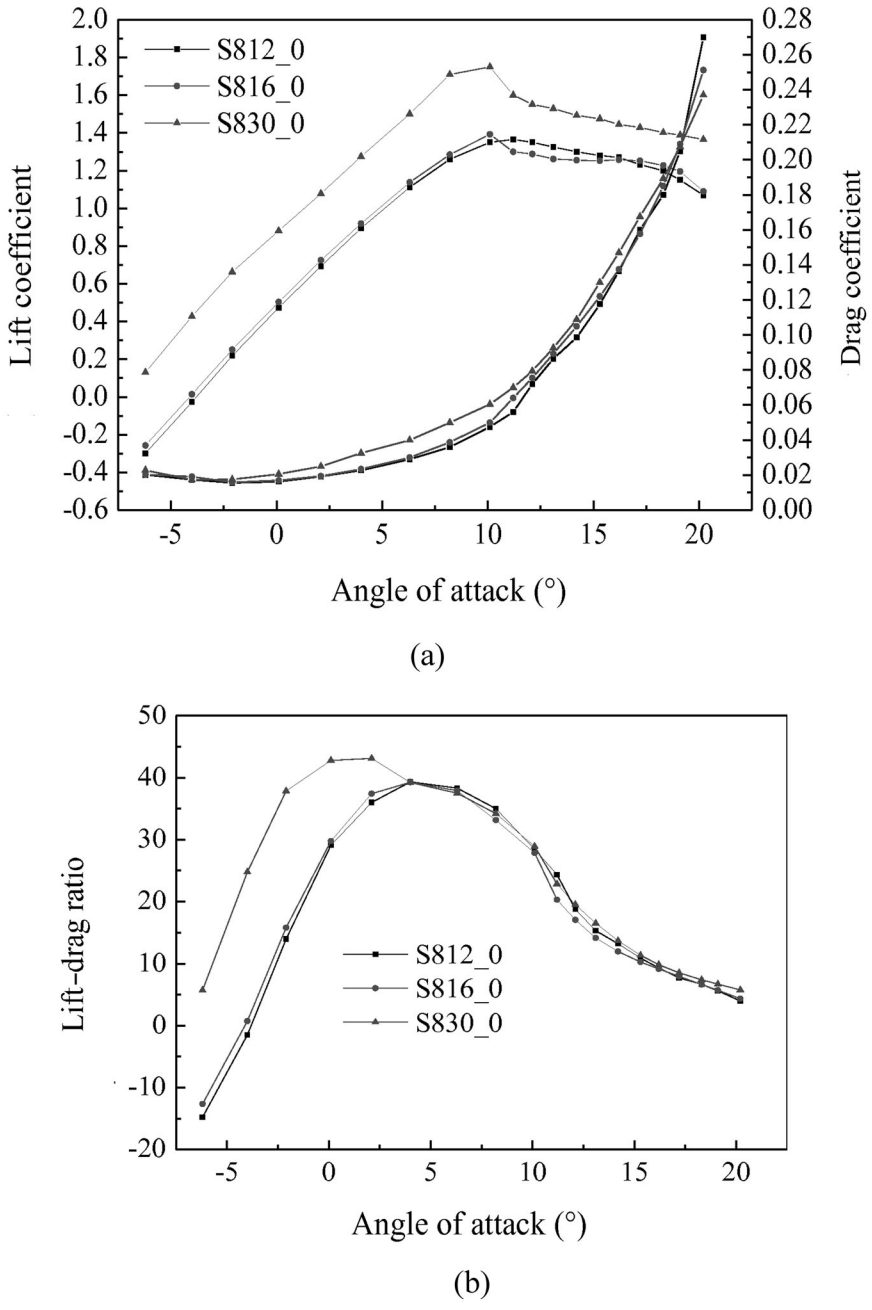

Fig. 11. Results of asymmetrical blunt trailing-edge airfoils with different relative cambers.

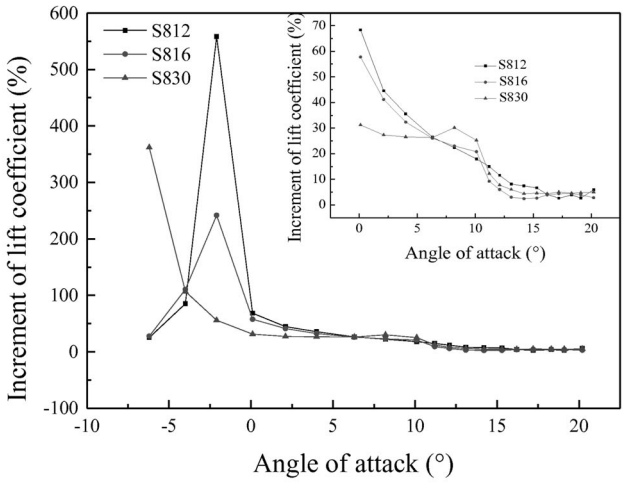

(a) Increment of lift coefficient

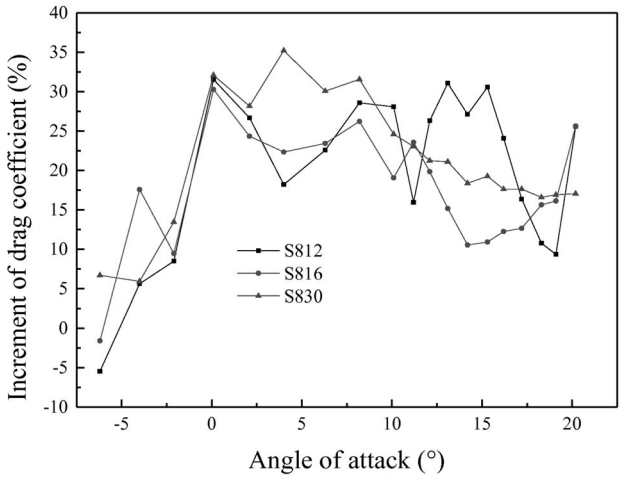

(b) Increment of drag coefficient

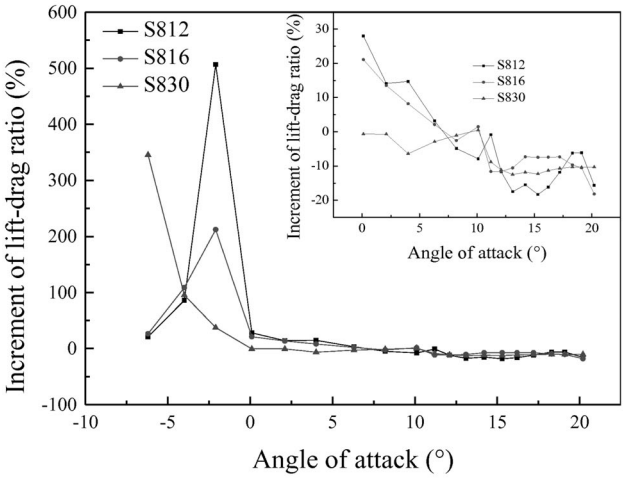

(c) Increment of lift-drag ratio

Fig. 12. Increment curves of airfoils with different relative cambers.

coefficients of S812_0 and S816_0 airfoils are very close and basically less than that of S830_0 airfoil. According to Fig. 11b, the lift–drag ratio increases with the increase of relative camber for the angle of attack less than 4°, and shows little change as the angle of attack exceeds 4°.

5.3. Effect of Relative Camber on Aerodynamic Performance Improvement of Asymmetrical Blunt Trailing-Edge Modification

Through analysis of the increments of lift and drag coefficients and lift–drag ratio, the effect of relative camber on the aerodynamic performance improvement of asymmetrical blunt trailing-edge modification is obtained, as shown in Fig. 12. *Inc*, the increment of aerodynamic parameter, can be defined as:

$$Inc = (val_{am} - val_{bm}) \times 100\%/val_{bm}, \tag{2}$$

where val_{bm} and val_{am} are the values of aerodynamic parameter before and after the modification, respectively.

Figure 12a shows that the lift coefficient increment is almost positive. And with the increase of relative camber, the lift coefficient increment decreases for the angle of attack less than 6.3°, and increases as the angle of attack is between 6.3° and 10.1° or exceeds 16.3°, but decreases first and then increases at different angles of attack ranging from 10.1° to 16.3°. It can also be observed from the graph that the lift coefficient increments of S812 and S816 airfoils are kept consistent basically for the angle of attack being between 0.1° and 20.2°, and are obviously higher or smaller than that of S830 airfoil for the angle of attack less than 6.3° or ranging from 6.3° to 11.2°, and are close to that of S830 airfoil as the angle of attack exceeds 11.2°.

In Fig. 12b, the drag coefficient increments of S812 and S816 airfoils show little change with the increase of relative camber and are basically smaller than that of S830 airfoil for the angle of attack less than 0.1°. As the angle of attack exceeds 0.1°, the drag coefficient increment of S812, S816, and S830 airfoils basically decreases first and then increases, and those of S816 and S830 airfoils mainly decrease with the angle of attack. The average increment of S812 airfoil is the largest, and is 23.3%.

According to Fig. 12c, with the increase of relative camber, the lift–drag ratio increment decreases for the angle of attack less than 6.3°, and basically increases first and then decreases as the angle of attack exceeds 6.3°. It can also be seen from the graph that the lift–drag ratio increments of S812 and S816 airfoils increase first and then decrease with the angle of attack, and the average increments of these two airfoils are −4.52% and −3.6% at different angles of attack ranging from 0.1° to 20.2°, respectively. The increment of S830 airfoil decreases with the angle of attack, and is positive for the angle of attack less than 0.1°, but quickly decreases and is basically negative for the angle of attack more than 0.1°. The minimum increment of S830 airfoil is −12.46% and appears around the angle of attack of 13.1°, and the average increment at different angles of attack ranging from 0.1° to 20.2° is −7.53%. Thus, on the whole, the average lift–drag ratio increment of S816 airfoil with the relative camber of 1.81% is the largest, and that of large camber airfoil S830 is the smallest. And the lift–drag ratio increment of S830 airfoil is negative as the angle of attack exceeds 0.1°. This shows the large camber airfoil is not suited to the asymmetrical blunt trailing-edge modification. In other words, we can achieve the best aerodynamic performance improvement of airfoil before the relative camber increases to a certain value. And it is not that the larger the relative camber is, the better the performance improvement is.

6. CONCLUSIONS

A numerical study has been developed to evaluate the effect of relative camber on the aerodynamic performance improvement of asymmetrical blunt trailing-edge modification. The simulation results of lift and drag coefficients of S812 airfoil are compared with experiment data, which shows good agreement and suggests that, the k-ω SST model can calculate the aerodynamic performance of airfoil very well.

Next, the modifications with different trailing-edge thicknesses and distribution ratios are obtained using the established expression of blunt trailing-edge modification profile, and the best trailing-edge thickness and thickness distribution ratio are investigated. It is observed that as the trailing-edge thickness increases, the lift and drag coefficients of S812_0, S812_1, and S812_2 airfoils increase and are higher than those of S812 airfoil. The lift coefficients of S812_3 and S812_4 airfoils are basically

smaller than that of S812 airfoil, and the drag coefficients are very close to that of S812 airfoil. Moreover, for the same trailing-edge thickness, the lift and drag coefficients decrease with the decrease of the trailing-edge thickness of the lower surface. Based on these analyses, the authors therefore suggest the best trailing-edge thickness of 2% c and thickness distribution ratio being 0:4 should be adopted in the blunt trailing-edge modification.

Finally, the relative camber effect analysis was done for the aerodynamic performance improvement of asymmetrical blunt trailing-edge modification with the best trailing-edge thickness and distribution ratio. It has been shown that as the relative camber increases, the lift coefficient increments of S812 and S816 airfoils show little change basically, and are obviously higher than or close to that of S830 airfoil for the angle of attack less than 6.3° or exceeding 11.2°, respectively. The drag coefficient increment basically decreases first and then increases for the angle of attack more than 0.1°, and the average increment of S812 airfoil is the largest and is 23.3%. The lift–drag ratio increment decreases for the angle of attack less than 6.3°, and basically increases first and then decreases for the angle of attack more than 6.3°, and that of S830 airfoil is basically negative as the angle of attack exceeds 0.1°. The average lift–drag ratio increments of S812, S816, and S830 airfoils are −4.52%, −3.6%, and −7.53% at different angles of attack ranging from 0.1° to 20.2°, respectively. Therefore, the medium camber airfoil is more suited to the asymmetrical blunt trailing-edge modification.

ACKNOWLEDGMENTS

This work was supported by the Natural Science Foundation of Tianjin (projects no. 17JCY-BJC20800 and 15JCYBJC48600) and by the Opening Funds of State Key Laboratory of Building Safety and Built Environment (project no. BSBE2014-08).

REFERENCES

1. Li, X.X., Yang, K., Zhang, L., Bai, J.Y., and Zhao, X.L., Design of Large Thickness Airfoil with Blunt Trailing Edge, *J. Eng. Therm.*, 2014, vol. 35, no. 9, pp. 1744–1748.
2. Roth-Johnson, P., Wirz, R.E., and Lin, E., Structural Design of Spars for 100-m Biplane Wind Turbine Blades, *Renew. Energ.*, 2014, vol. 71, pp. 133–155.
3. Andersen, P.B., Gaunaa, M., Bak, C., and Buhl, T., Load Alleviation on Wind Turbine Blades Using Variable Airfoil Geometry, *Wind Eng.*, 2005, vol. 29, no. 2, pp. 169–182.
4. Mayda, E.A., van Dam, C.P., Chao, D.D., and Berg, D.E., *Computational Design and Analysis of Flatback Airfoil Wind Tunnel Experiment*, Albuquerque: Sandia National Laboratories, 2008.
5. Jackson, K.J., Zuteck, M.D., van Dam, C.P., Standish, K.J., and Berry, D., Innovative Design Approaches for Large Wind Turbine Blades, *Wind Eng.*, 2005, vol. 8, no. 2, pp. 141–171.
6. Baker, J.P., Mayda, E.A., and van Dam, C.P., Experimental Analysis of Thick Blunt Trailing-Edge Wind Turbine Airfoils, *J. Sol. Eng.-T ASME*, 2006, vol. 128, no. 4, pp. 422–431.
7. Standish, K.J. and van Dam, C.P., Aerodynamic Analysis of Blunt Trailing Edge Airfoils, *J. Sol. Eng.-T ASME*, 2003, vol. 125, no. 4, pp. 479–487.
8. Singh, R.K., Rafiuddin Ahmed, M., and Zullah, A., Design of a Low Reynolds Number Airfoil for Small Horizontal Axis Wind Turbines, *Renew. Eng.*, 2012, vol. 42, pp. 66–76.
9. Singh, R.K. and Rafiuddin Ahmed, M., Blade Design and Performance Testing of a Small Wind Turbine Rotor for Low Wind Speed Applications, *Renew. Eng.*, 2013, vol. 50, pp. 812–819.
10. Chao, D.D. and van Dam, C.P., Computational Aerodynamic Analysis of a Blunt Trailing-Edge Airfoil Modification to the NREL Phase VI Rotor, *Wind Eng.*, 2007, vol. 10, no. 6, pp. 529–550.
11. Deng, L., Qiao, Z.D., Yang, X.D., and Xiong, J.T., Aerodynamics Performance Computational of Trailing-Edge-Blunting Methods of Flatback Airfoil for Large Wind Turbine Based on RANS Equation, *Acta Energiae Solaris Sinica*, 2012, vol. 33, no. 4, pp. 545–551.
12. Xu, H.R., Yang, H., and Liu, C., Numerical Value Analysis on Aerodynamic Performance of DU Series Airfoils with Thickened Trailing Edge, *Transact. Chinese Soc. Agricult. Eng.*, 2014, vol. 30, no. 17, pp. 101–108.
13. Li, R.N., Yuan, S.K., and Zhao, Z.Q., Research on the Effect of Trail-Edge Improvement on Airfoils Performance for Wind Turbine, *Acta Aerodynam. Sinica*, 2012, vol. 30, no. 5, pp. 646–652.
14. Shen, Z.H. and Yu, G.L., Influence of Airfoil's Camber on the Performance of Wind Turbines, *J. Power Eng.*, 2007, vol. 27, no. 1, pp. 136–139.
15. Shen, Z.H., Yu, G.L., Shen, H.Y., and Zhu, W.X., The Experimental Study of Enhancement of Wind Turbine Performance by Increasing Blade Camber, *Acta Energiae Solaris Sinica*, 2007, vol. 28, no. 8, pp. 830–833.

16. Larsen, J.W., Nielsena, S.R.K., and Krenk, S., Dynamic Stall Model for Wind Turbine Airfoils, *J. Fluid Struct.*, 2007, vol. 23, pp. 959–982.
17. Li, R.N., Zhang, S.A., Yang, R., and Li, D.S., Effect of Aerofoil Camber on Airfoil Aerodynamic Performance, *Fluid Machin.*, 2009, vol. 37, no. 5, pp. 17–21.
18. Chen, J., Wang, Q., Pang, X.P., Li, S.L., and Guo, X.F., Improvement of Airfoil Design Using Smooth Curvature Technique, *Renew. Eng.*, 2013, vol. 51, pp. 426–435.
19. Mohamed, M.H., Ali, A.M., and Hafiz, A.A., CFD Analysis for H-Rotor Darrieus Turbine as a Low Speed Wind Energy Converter, *Eng. Sci. Technol. Int. J.*, 2015, vol. 18, no. 1, pp. 1–13.
20. Yang, H., Shen, W.Z., Xu, H.R., Hong, Z.D., and Liu, C., Prediction of the Wind Turbine Performance by Using BEM with Airfoil Data Extracted from CFD, *Renew. Eng.*, 2014, vol. 70, pp. 107–115.
21. Choudhry, A., Arjomandi, M., and Kelso, R., A Study of Long Separation Bubble on Thick Airfoils and Its Consequent Effects, *Int. J. Heat Fluid Fl.*, 2015, vol. 52, pp. 84–96.
22. Ramsay, R.R. and Gregorek, G.M., *Effects of Grit Roughness and Pitch Oscillations on the S812 Airfoil*, Golden, Colorado: National Renewable Energy Laboratory, 1998.
23. Li, C., Zhu, S.Y., Xu, Y.L., and Xiao, Y.Q., 2.5D Large Eddy Simulation of Vertical Axis Wind Turbine in Consideration of High Angle of Attack Flow, *Renew. Eng.*, 2013, vol. 51, pp. 317–330.
24. Pauley, L.L., Moin, P., and Reynolds, W.C., The Structure of Two-Dimensional Separation, *J. Fluid Mech.*, 1990, vol. 220, pp. 397–411.